

Robust Lower Bounds on Magnetic Fields in Intergalactic Voids from Long-Term GeV-TeV Light Curves of the Blazar Mrk 421

Keitaro Takahashi^{1,7}, Masaki Mori², Kiyotomo Ichiki³, Susumu Inoue^{4,5}, Hajime Takami⁶,

ABSTRACT

Lower bounds are derived on the amplitude B of intergalactic magnetic fields (IGMFs) in the region between our Galaxy and the blazar Mrk 421, from constraints on the delayed GeV flux of pair echos that are emitted by secondary e^-e^+ produced in $\gamma\gamma$ interactions between primary TeV gamma-rays and the cosmic infrared background. The distribution of galaxies mapped by the Sloan Digital Sky Survey shows that this region is dominated by a large intergalactic void. We utilize data from long-term, simultaneous GeV-TeV observations by the *Fermi* Large Area Telescope and the ARGO-YBJ experiment extending over 600 days. For an assumed value of B , we evaluate the daily GeV flux of the pair echo expected from the TeV data, select the dates where this exceeds the *Fermi* 2- σ sensitivity, compute the probability that this flux is excluded by the *Fermi* data for each date, and then combine the probabilities using the inverse normal method. Consequently, we exclude $B < 10^{-20.5}$ G for a field coherence length of 1 kpc at $\sim 4\text{-}\sigma$ level. This is much more significant than the 2- σ bounds we obtained previously from observations of Mrk 501 involving Cherenkov telescopes, by virtue of more extensive data and improved statistical analysis. Compared with most other studies of IGMF bounds, the evidence we present here for a non-zero IGMF is more robust as it does not rely on unproven assumptions on the primary TeV emission during unobserved periods.

Subject headings: magnetic fields — gamma rays: observations — galaxies: active — gamma rays: theory — BL Lacertae objects: individual (Mrk 421) — radiation mechanisms: nonthermal

1. Introduction

Intergalactic magnetic fields (IGMF), especially those inside intergalactic void regions, have attracted much attention because they could be a remnant of phenomena that generated primordial magnetic fields in the early Universe (e.g. Gnedin et al. 2000; Langer et al. 2005; Takahashi et al. 2005; Ichiki et al. 2006). While primordial magnetic fields can be amplified later within galaxies and galaxy clusters by dynamo processes, they may remain unaffected by subsequent astrophysical effects deep inside voids. Thus, IGMFs are expected to be a window onto the early Universe. For comprehensive reviews on primordial and intergalactic magnetic fields, see Widrow (2002), Widrow et al. (2012) and Ryu et al. (2012).

However, the predicted amplitudes of primor-

dial magnetic fields are generally very small, $B = 10^{-25} - 10^{-15}$ Gauss, and difficult to probe with methods such as Faraday rotation of distant radio sources or the anisotropy of cosmic microwave background. In this context, a novel method utilizing delayed secondary emission from high-energy gamma-ray sources was proposed by Plaga (1995) and subsequently developed by many authors (Dai et al. 2002; Razzaque et al. 2004; Murase et al. 2007; Murase et al. 2008; Ichiki et al. 2008; Takahashi et al. 2008; Elyiv et al. 2009; Neronov & Semikoz 2009; Takahashi et al. 2011). This emission that we refer to as “pair echo” is expected to occur typically at GeV energies, for which the *Fermi* Large Area Telescope (LAT) provides important constraints. Since the echo flux is predicted to be larger for smaller B , a GeV upper limit translates into a lower bound on B .

In our previous study (Takahashi et al. 2012),

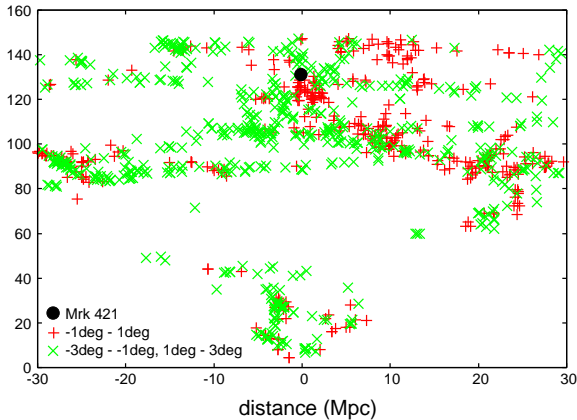


Fig. 1.— Distribution of galaxies between Mrk 421 and our Galaxy mapped by SDSS. The pluses and crosses represent galaxies located within a 1-degree slice and a 3-degree slice (but outside the 1-degree slice) from the plane with declination 38.2, respectively. The width of 1-degree slice is about 1.7 Mpc at 100 Mpc from our Galaxy.

we focused on a specific TeV flare of Mrk 501 observed in 2009 by the VERITAS (Very Energetic Radiation Imaging Telescope Array System) and MAGIC (Major Atmospheric Gamma-ray Imaging Cherenkov) telescopes. Calculating the lightcurve of the pair echo expected from the flare and the quiescent emission before and after the flare and comparing with simultaneous *Fermi* observations, we obtained a lower bound on the IGMF of $B > 10^{-20}$ Gauss (90% C.L.) for a field coherence length of 1 kpc. Being based firmly on the observational data and nearly free of assumptions concerning the primary TeV flux in unobserved periods or spectral bands, our result is more robust compared to previous studies (Neronov & Vovk 2010; Ando & Kusenko 2010; Tavecchio et al. 2011; Tavecchio et al. 2010; Dolag et al. 2011; Dermer et al. 2011; Neronov et al. 2011; Taylor et al. 2011; Arlen et al. 2012).

Here we focus on the TeV blazar Mrk 421 located at $z = 0.031$. As seen in Fig. 1, maps of the local galaxy distribution from the Sloan Digital Sky Survey reveal that a huge void lies between our galaxy and the supercluster containing Mrk 421 (Abazajian et al. 2009; Blanton et al. 2005). This is also seen to be the case for Mrk 501. Thus, Mrk 421 is a desirable target for probing

IGMFs. Mrk 421 has been monitored continuously at TeV energies by the ARGO-YBJ experiment over the period from 2007 November to 2010 February (Bartoli et al. 2011), during which many flares were observed so that more statistically significant bounds on IGMFs can be expected. Note that compared to Cherenkov telescopes, such air shower detectors have a much higher duty cycle and allow uninterrupted long-term observations, albeit at lower sensitivity.

2. TeV and GeV Emission from Mrk 421

For the calculation of pair echo, we need the spectrum and lightcurve of TeV emission. In Bartoli et al. (2011), the daily fluxes above 0.3 TeV are given for about 1000 days. Among them some negative daily fluxes are reported. They would be due to the systematic error and we simply set them zero. Although the daily spectra are not given, the average spectra were derived from four flux-level data groups according to the X-ray counting rate. In this letter, because the X-ray data is not available, we divide the data into three groups according to the TeV daily count. This is justified because the TeV count was shown to be tightly correlated with the X-ray count rate. Our three groups, "high" (TeV daily count > 80), "medium" ($80 > \text{TeV daily count} > 40$) and "low" (TeV daily count < 40), correspond to the X-ray flux levels 4, 3 and 2 (level 1 has almost the same spectral index with that of level 2 so low state includes level 1 as well), respectively. We adopt the spectral indices given by Bartoli et al. (2011) and scale the normalization with the flux day by day according to the corresponding group. Minimum and maximum cutoffs are also imposed at 0.1 TeV and 5 TeV, respectively, the latter corresponding to the highest energy photons detected by ARGO-YBJ.

Fig. 2, absorbed and unabsorbed spectra of the three groups are shown. Here the absorbed spectra are calculated using the CIB model of Franceschini et al. (2008), which was also adopted in Bartoli et al. (2011). It turns out that most of constraints on IGMF come from the emission during high state and low state does not affect the result at all.

On the other hand, concerning GeV gamma-rays, *Fermi* LAT has performed uninterrupted monitoring of Mrk 421 in the survey mode from MJD 54683. The data were acquired via the *Fermi*

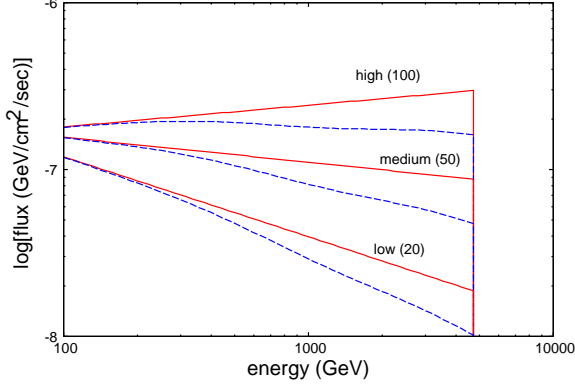


Fig. 2.— The unabsorbed (solid) and absorbed (dashed) spectra of Mrk 421 for the high, medium and low states (from top to bottom). The values in the parentheses indicate the daily TeV count.

Science Support Center (FSSC). We use the standard analysis tools supplied by FSSC in three energy bands, 100 MeV–1 GeV, 1–10 GeV, and >10 GeV, so as to keep reasonable photon statistics in time intervals as short as one day while retaining some energy resolution. Since the statistics are still small, we adopted the aperture photometry method, i.e., events falling within one degree from the source were counted. Note that background events above 1 GeV in one-day bins at the high Galactic latitude of Mrk 421 are essentially negligible. Flux probability distribution functions were calculated assuming Poisson statistics when the data show no significant gamma-ray signal. Below we use data during MJD 54683–55255, when both TeV and GeV observations were performed. Also we focus on an energy range of 1–10 GeV for the pair echo, where *Fermi* LAT is the most sensitive to the pair echo.

3. Pair Echo

Here let us summarize briefly the basic physics of pair echo emission (see e.g. Ichiki et al. 2008 and Takahashi et al. 2012 for more details). Primary gamma-rays with energy $E_\gamma \gtrsim 1$ TeV emitted from an extragalactic source have mean free path $\lambda_{\gamma\gamma} = 1/(0.26\sigma_T n_{\text{IR}}) = 190 \text{ Mpc } (n_{\text{IR}}/0.01 \text{ cm}^{-3})^{-1}$ for $\gamma\gamma$ pair production interactions with photons of the cosmic infrared background (CIB), where σ_T is the Thomson cross section and n_{IR} is the number

density of CIB photons most relevant for the interactions. The produced pairs with energy $E_e \approx E_\gamma/2$ give rise to the pair echo emission by IC upscattering of ambient cosmic microwave background (CMB) photons to average energy $\langle E_{\text{echo}} \rangle = 2.7 T_{\text{CMB}} \gamma_e^2 = 2.5 \text{ GeV } (E_\gamma/2 \text{ TeV})^2$, where $\gamma_e = E_e/m_e c^2$ is the Lorentz factor of the pairs and $T_{\text{CMB}} = 2.7 \text{ K}$ is the CMB temperature. Thus, primary gamma-rays in the range $E_\gamma \simeq 1 - 5 \text{ TeV}$ induce echos with typical energies $E_{\text{echo}} \simeq 1 - 10 \text{ GeV}$. The pairs upscatter CMB photons successively until they lose most of their energy after propagating an IC cooling length $\lambda_{\text{IC,cool}} = 3m_e^2/(4E_e\sigma_T U_{\text{CMB}}) = 350 \text{ kpc } (E_e/1 \text{ TeV})^{-1}$, where U_{CMB} is the CMB energy density. The length scales for $\lambda_{\gamma\gamma}$ and $\lambda_{\text{IC,cool}}$ imply that the secondary pairs typically arise in locations far removed from the source on scales of intergalactic voids, whereas the pairs propagate only for short distances within such regions while generating the echo emission. In our case with Mrk 421, as we saw in Fig. 1, there is a huge void between our galaxy and Mrk 421 and, noting that the typical scattering angle of gamma-rays and charged particles is $\sim 1/\gamma_e \sim 10^{-6}$, their propagation region is mostly in the void space.

The pair echo emission arrives at the observer with a time delay relative to the primary emission, caused by the effects of angular spreading in pair production and IC interactions, as well as by deflections of the pairs in intervening magnetic fields. The typical delay time due to angular spreading is $\Delta t_{\text{ang}} = (\lambda_{\gamma\gamma} + \lambda_{\text{IC,cool}})/2\gamma_e^2 \approx 3 \times 10^3 \text{ sec } (E_{\text{echo}}/1 \text{ GeV})^{-1} (n_{\text{IR}}/0.01 \text{ cm}^{-3})^{-1}$ (Ichiki et al. 2008), while that due to magnetic deflections is $\Delta t_{\text{B}} = (\lambda_{\gamma\gamma} + \lambda_{\text{IC,cool}})\langle\theta_{\text{B}}^2\rangle/2$, where $\langle\theta_{\text{B}}^2\rangle^{1/2} = \max[\lambda_{\text{IC,cool}}/r_{\text{L}}, (\lambda_{\text{IC,cool}}r_{\text{coh}}/6)^{1/2}/r_{\text{L}}]$ is the variance of the magnetic deflection angle in terms of the Larmor radius r_{L} and field coherence length r_{coh} . If $r_{\text{coh}} \ll \lambda_{\text{IC,cool}}$,

$$\Delta t_{\text{B}} \approx 2 \times 10^4 \text{ sec } (E_{\text{echo}}/1 \text{ GeV})^{-3/2} (B/10^{-19} \text{ G})^2 \times (r_{\text{coh}}/1 \text{ kpc}) (n_{\text{IR}}/0.01 \text{ cm}^{-3})^{-1}, \quad (1)$$

where B is the field amplitude. Hereafter we fiducially take $r_{\text{coh}} = 1 \text{ kpc}$ (see e.g. Langer et al. 2005), but the results are scalable to other values of r_{coh} since it enters only through the combination $B^2 r_{\text{coh}}$ and only when $r_{\text{coh}} \lesssim \lambda_{\text{IC,cool}}$. The total delay time is approximately $\Delta t = \Delta t_{\text{ang}} + \Delta t_{\text{B}}$, and the magnetic field properties are reflected in

the delay as long as $\Delta t_{\text{ang}} \lesssim \Delta t_{\text{B}}$.

The spectra and light curves of the pair echo can be evaluated as follows. For a primary fluence dN_{γ}/dE_{γ} , the associated time-integrated flux of secondary pairs is

$$\frac{dN_{e,0}}{d\gamma_e}(\gamma_e) = 4m_e \frac{dN_{\gamma}}{dE_{\gamma}}(E_{\gamma} = 2m_e\gamma_e) \left[1 - e^{-\tau_{\gamma\gamma}(E_{\gamma}=2\gamma_em_e)} \right] \quad (2)$$

where $\tau_{\gamma\gamma}(E_{\gamma})$ is the $\gamma\gamma$ optical depth in the CIB. The time-dependent echo spectrum is

$$\frac{d^2 N_{\text{echo}}}{dt dE_{\gamma}} = \int d\gamma_e \frac{dN_e}{d\gamma_e} \frac{d^2 N_{\text{IC}}}{dt dE_{\gamma}}, \quad (3)$$

where $d^2 N_{\text{IC}}/dt dE_{\gamma}$ is the IC power from a single electron or positron, and $dN_e/d\gamma_e$ is the total time-integrated flux of pairs responsible for the echo emission observed at time t , related nontrivially to $dN_{e,0}/d\gamma_e$ in Eq. (2). In Takahashi et al. (2012), we developed a formalism to calculate this factor accounting for the finite probability of pair production near the observer, extending the earlier work by Dai et al. (2002).

Note that the pair echo fluence is determined by the total amount of absorbed primary gamma rays and thus independent of the IGMF, in contrast to the pair-echo flux which is roughly given by the fluence divided by Δt . Weaker IGMFs generally give higher echo fluxes, as long as the time delay does not become dominated by angular spreading and the echo flux remains sensitive to B . For $r_{\text{coh}} = 1$ kpc, Δt_{B} approaches Δt_{ang} if $B \sim 10^{-20}$ G. This behavior is clearly seen in Fig. 3 which shows the lightcurves of pair echo with 1–10 GeV and TeV daily counts. Pair-echo flux rises on the occasion of TeV emission and decays in the absence of it. For smaller IGMF the response to TeV emission is quicker and the peak flux is larger. Finally, here, we do not consider the possibility that the pairs lose energy by heating the intergalactic gas through plasma instabilities (Broderick et al. 2012), as the efficiency of this process has been disputed (Miniati & Elyiv 2012) and is highly uncertain.

4. Statistical Analysis

In this section, we compare the calculated pair-echo flux with the *Fermi*-LAT data and derive constraints on IGMF. In contrast to the previous

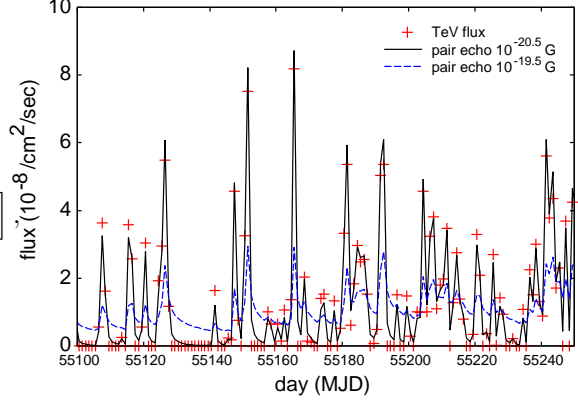


Fig. 3.— Expected lightcurves of the pair echo in the 1–10 GeV band (solid and dashed lines for $B = 10^{-20.5}, 10^{-19.5}$ Gauss, respectively) compared with the observed TeV lightcurve (points, arbitrary units).

paper (Takahashi et al. 2012), we have vast numbers of independent flux bins (each bin represents the daily flux) so we need a more sophisticated way to derive constraints. First, we compute the probability P_i that a specific value of IGMF amplitude is excluded by the i -th flux bin, using the probability distribution function of the true flux obtained from *Fermi*-LAT observation. Then, we combine the probabilities to derive the total probability P_{tot} using meta-analysis.

Here, it should be noted that it is not appropriate to combine probabilities from all bins. The reason is as follows. If the TeV emission is very weak for the i -th bin, the expected pair-echo flux on that bin is very low irrespective of the value of IGMF. Consequently, given an upper bound on GeV flux by *Fermi*, the probability P_i would become very small. If we combine such P_i s, the total probability P_{tot} would also become very small, that is, any values of IGMF would not be excluded even if some P_i s are very large at TeV flares. In fact, it is not fair to combine P_i s of time bins where the pair-echo fluxes are expected to be much smaller than the *Fermi* sensitivity because it is natural for the pair echo not to be observed and *Fermi* data would not have any information on IGMF. Thus, we need to choose data bins where the pair echo should have been observed. Note that the data bins which should be chosen depends on the value of IGMF because the pair-echo flux

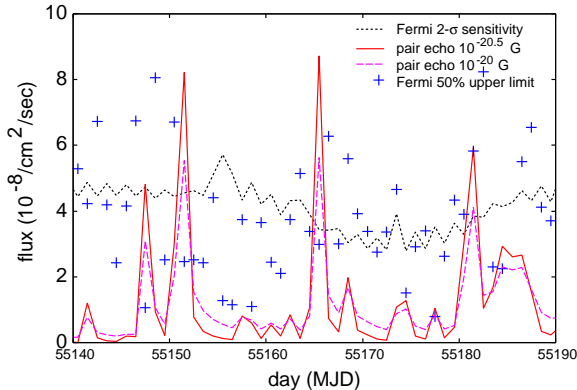


Fig. 4.— *Fermi*-LAT 2- σ daily sensitivity (dotted), lightcurves of pair echo with $B = 10^{-20.5}$ Gauss (solid) and $B = 10^{-20}$ Gauss (dashed) and *Fermi* 50% upper limits (points). All are for an energy range of 1 – 10 GeV.

depends on it. In general, as we explained above, larger IGMF results in a lower flux so that the pair echo is harder to be observed and the number of chosen data bins would be smaller.

In this letter, we set a threshold to choose data bins such that the expected pair-echo flux exceeds the 2- σ sensitivity of *Fermi*-LAT. In Fig. 4, the 2- σ sensitivity and the pair-echo lightcurves for $B = 10^{-20.5}$ Gauss and $B = 10^{-20}$ Gauss are plotted for an energy range of 1 – 10 GeV. As can be seen, during this period (which is only a small part of the whole period), 4 and 3 bins exceed the *Fermi*-LAT sensitivity in cases with $B = 10^{-20.5}$ Gauss and $B = 10^{-20}$ Gauss, respectively. Looking back at Fig. 3, large TeV flares can be seen at these selected bins.

In Fig. 4, the 50% upper limits on the daily flux are also plotted. Looking at the first flare at MJD 55147, the *Fermi*-LAT upper limit is much smaller than the expected pair-echo flux for $B = 10^{-20.5}$ Gauss so that the probability that this value of IGMF is excluded is very large. On the other hand, for $B = 10^{-20}$ Gauss, the pair-echo flux does not exceed the sensitivity and this bin is not counted to compute P_{tot} , even though the pair-echo flux is larger than the upper limit. As to the second (MJD 55152) and third (MJD 55166) flares, the pair-echo fluxes are larger than the upper limits both for $B = 10^{-20.5}$ Gauss and 10^{-20} Gauss. At the fourth flare (MJD 55182),

the pair-echo flux for $B = 10^{-20.5}$ Gauss is almost the same as the upper limit. Because this is the 50% upper limit, this bin does not favor or exclude this value of IGMF. On the other hand, in the case with $B = 10^{-20}$ Gauss, the pair-echo flux is smaller than the upper limit and this value of IGMF is allowed.

In this way, for a specific value of IGMF, appropriate bins are chosen and the expected pair-echo flux is compared with the *Fermi*-LAT data. Here, we consider the probability distribution function of the true flux and calculate the probability, P_i , that the true flux is below the pair-echo flux for the i -th bin. Then, to combine P_i s, we use the inverse normal method, which is a kind of meta-analysis as we explain below. First, derive the Z value of the normal distribution for the i -th bin, Z_i , which corresponds to the percentile (point) of the one-sided P value P_i . It should be noted that Z_i is negative if $P_i < 0.5$. Second, compute the total Z value Z_{tot} by the following equation,

$$Z_{\text{tot}} = \frac{1}{\sqrt{N}} \sum_{i=1}^N Z_i, \quad (4)$$

where N is the number of the selected bins. Finally, derive the one-sided P value P_{tot} of the normal distribution which corresponds to the above Z_{tot} . Thus, we can interpret this P_{tot} such that this value of IGMF is excluded at the confidence level P_{tot} .

Fig. 5 shows the Z value Z_{tot} as a function of the IGMF amplitude. Because the time delay Δt is dominated by the angular spreading time for $B \leq 10^{-20.5}$ Gauss, the result does not change for that range and such a weak IGMF including zero IGMF is excluded by about 4- σ significance. The significance decreases for larger IGMFs and a IGMF larger than $10^{-19.7}$ Gauss is not constrained at all. This is because the pair-echo flux is strongly dependent on the IGMF value and there are no bins where the pair-echo flux exceeds the threshold for $B \geq 10^{-19.5}$ Gauss.

Finally, it is noticed that we assumed there is no emission in GeV range other than the pair echo. In fact, there must be the primary GeV emission and possibly some other emission. If we could know their existence and the amount somehow, the constraints on the pair echo would become tighter, given the same upper limit on the GeV emission

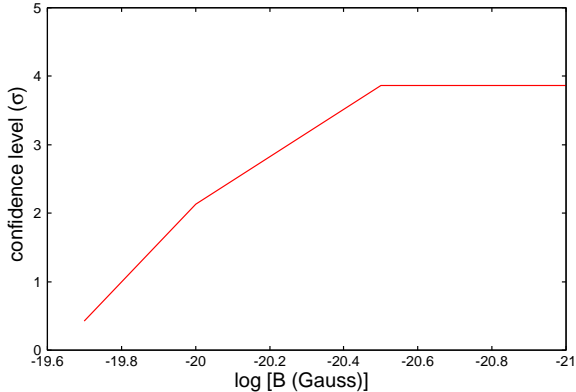


Fig. 5.— The Z value Z_{tot} that the value of IGMF is excluded by the *Fermi* data.

by *Fermi*-LAT. In this letter, we consider only pair echo for GeV emission, which leads to conservative constraints on the amount of pair echo and then IGMF.

5. Discussion and Summary

Using data from simultaneous GeV-TeV observations of Mrk 421 by *Fermi*-LAT and ARGO-YBJ, we constrained the GeV flux of pair echos and derived lower bounds on the IGMF strength inside a large void region located between our Galaxy and Mrk 421. This was done by: 1) calculating the daily pair-echo flux from the TeV data over 600 days, 2) selecting the dates where the expected pair-echo flux exceeds the *Fermi*-LAT $2\text{-}\sigma$ sensitivity, 3) computing the probability that an assumed value of the IGMF is excluded by the *Fermi*-LAT data for each date, and 4) combining these probabilities to derive the total probability using the inverse normal method. Consequently, an IGMF weaker than $10^{-20.5}$ Gauss for a field coherence length of 1 kpc is excluded by about $4\text{-}\sigma$. The result can be roughly scaled for other values of r_{coh} as $B \gtrsim 10^{-22} \max[(r_{\text{coh}}/350 \text{ kpc})^{-1/2}, 1] \text{ G}$.

As with our previous analysis using Mrk 501 (Takahashi et al. 2012), no assumptions are made here concerning the TeV emission during unobserved periods. The obtained constraints are thus more robust compared to other studies, in particular those based on limits to the spatially-extended halo emission from secondary pairs that inevitably involves very long time delays, often

longer than the typical lifetimes of blazars. Although the value of the lower limit obtained here is similar to our previous work, the statistical significance has improved remarkably, from less than $2\text{-}\sigma$ to about $4\text{-}\sigma$, thanks to the much larger data and improved statistical analysis.

Here we used the *Fermi*-LAT data only as upper limits to the GeV fluxes. Because the pair-echo flux is strongly dependent on the TeV flux, we can potentially obtain tighter constraints on the IGMF by searching for statistical correlations between the *Fermi*-LAT data and ARGO-YBJ data. This will be presented elsewhere in near future.

We thank Songzhan Chen who kindly provided us with the ARGO-YBJ data. This work is supported in part by the Grant-in-Aid from the Ministry of Education, Culture, Sports, Science and Technology (MEXT) of Japan, No. 23740179, No. 24111710 and No. 24340048 (KT), No. 22540315 (MM), No. 24340048 (KI) and No. 22540278 (SI), and by the Grant-in-Aid for the global COE program “Quest for Fundamental Principles in the Universe: from Particles to the Solar System and the Cosmos” at Nagoya University from MEXT of Japan. The work of HT is supported by JSPS fellowship.

REFERENCES

- Abazajian, K. N., et al. 2009, *ApJS* 182, 543
- Ando, S., & Kusenko, A. 2010, *ApJ*, 722, L39
- Arlen, T. C., Vassiliev, V. V., Weisgarber, T., Wakely, S. P., & Yusef Shafi, S., *ArXiv eprints*, 1210.2802
- Blanton, M., et al. 2005 *AJ*, 129, 2562
- Bartoli, B., et al. 2011, *ApJ*, 734, 110
- Broderick, A. E., Chang, P., & Pfrommer, C. 2012, *ApJ*, 752, 22
- Dai, Z. G., Zhang, B., Gou, L. J., Mészáros, P., & Waxmann, E. 2002, *ApJL*, 580, L7
- Dermer, C. D., Cavadini, M., Razzaque, S., Finke, J. D., & Lott, B. 2011, *ApJL*, 733, L21
- Dolag, K., Kachelrieß, M., Ostapchenko, S., & Tomás, R. 2011, *ApJL*, 727, L4

- Elyiv, A., Neronov, A., & Semikoz, D. V. 2009 Phys. Rev. D, 80 023010
- Franceschini, A., Rodighiero, G., & Vaccari, M. 2008, A&A, 487, 837
- Gnedin, N. Y., Ferrara, A. & Zweibel, E. 2000, ApJ, 539, 505
- Ichiki, K., Inoue, S., & Takahashi, K. 2008, ApJ, 682, 127
- Ichiki, K., Takahashi, K., Ohno, H., Hanayama, H., & Sugiyama, N. 2006, Science, 311, 827
- Langer, M., Aghanim, N., & Puget, J.-L. 2005, A&A, 443, 367
- Miniati, F. & Elyiv, A. 2012, arXiv:1208.1761
- Murase, K., Asano, K., & Nagataki, S. 2007, ApJ, 671, 1886
- Murase, K., Takahashi, K., Inoue, S., Ichiki, K., & Nagataki, S. 2008, ApJ, 686, L67
- Neronov, A., & Semikoz, D. V. 2009, Phys. Rev. D, 80, 123012
- Neronov, A., Semikoz, D. V., Tinyakov, P. G., & Tkachev, I. I. 2011, A&A, 526, A90
- Neronov, A., & Vovk, I. 2010, Science, 328, 73
- Plaga, R. 1995, Nature, 374, 430
- Razzaque, S., Mészáros, P., & Zhang, B. 2004, ApJ, 613, 1072
- Ryu, D., Schleicher, D. R. G., Treumann, R. A., Tsagas, C. G., & Widrow, L. M. 2012, Space Science Reviews, 166, 1
- Takahashi, K., Ichiki, K., Ohno, H., & Hanayama, H. 2005, Phys. Rev. Lett., 95, 121301
- Takahashi, K., Inoue, S., Ichiki, K., & Nakamura, T. 2011, MNRAS, 410, 2741
- Takahashi, K., Mori, M., Ichiki, K., & Inoue, S. 2012, ApJL, 744, L7
- Takahashi, K., Murase, K., Ichiki, K., Inoue, S., & Nagataki, S., 2008, ApJ, 687, L5
- Tavecchio, F., Ghisellini, G., Bonnoli, G., & Foschini, L. 2010a, ArXiv e-prints, 2011, MNRAS, 414, 3566
- Tavecchio, F., Ghisellini, G., Foschini, L., Bonnoli, G., Ghirlanda, G., & Coppi, P. 2010, MNRAS, 406, L70
- Taylor, A. M., Vovk, I., & Neronov, A. 2011, A&A, 529, 9
- Widrow, L. M. 2002, Reviews of Modern Physics, 74, 775
- Widrow, L. M., Ryu, D., Schleicher, D. R. G., Subramanian, K., Tsagas, C. G., & Treumann, R. A. 2012, Space Science Reviews, 166, 37